Photonics **2015**, *2*, 459-467; doi:10.3390/photonics2020459

OPEN ACCESS

photonics

ISSN 2304-6732

www.mdpi.com/journal/photonics

Article

FDTD for Hydrodynamic Electron Fluid Maxwell Equations

Yingxue Zhao * and Jinjie Liu

Department of Mathematical Sciences, Delaware State University, 1200 N. Dupont Hwy, Dover, DE 19901, USA; E-Mail: jliu@desu.edu

* Author to whom correspondence should be addressed; E-Mail: yzhao112@students.desu.edu; Tel.: 001-302-857-7051

Received: 15 April 2015 / Accepted: 4 May 2015 / Published: 6 May 2015

Abstract: In this work, we develop a numerical method for solving the three dimensional hydrodynamic electron fluid Maxwell equations that describe the electron gas dynamics driven by an external electromagnetic wave excitation. Our numerical approach is based on the Finite-Difference Time-Domain (FDTD) method for solving the Maxwell's equations and an explicit central finite difference method for solving the hydrodynamic electron fluid equations containing both electron density and current equations. Numerical results show good agreement with the experiment of studying the second-harmonic generation (SHG) from metallic split-ring resonator (SRR).

Keywords: second-harmonic generation; hydrodynamic electron fluid Maxwell equations; split-ring resonator

1. Introduction

Maxwell's equations are a set of partial differential equations governing the electromagnetic (EM) waves [1]. Solution to the Maxwell's equations is very important for studying many physical phenomena. Among many methods for solving Maxwell's equations, the Finite-Difference Time-Domain (FDTD) method is one of the most popular numerical approaches [2]. Here, we numerically investigate the solution of Maxwell's equations in nonlinear media and its application to nonlinear optics.

Recently, experiments have shown that strong nonlinear response such as the second-harmonic wave can be generated from Split-Ring Resonator (SRR) [3–6]. The SRR consists of array of

U-shaped metallic gold nanoparticles. Under the excitation of an external electromagnetic wave, strong nonlinear optical wave is generated. A classical theory based on the cold plasma Maxwell's equations are developed in [6–8] to study the nonlinear optical response for this structure. In [6,7], perturbation expansion of nonlinearities is used in order to solve the cold plasma-Maxwell's equations. In [8], a nonlinear Drude model is developed and solved by a time-splitting finite difference method. In [9,10], full fluid equations (Euler's equations) are coupled to the Maxwell's equations and is solved by perturbation expansion of nonlinearities. In [11], the discontinuous Galerkin time domain method and the hydrodynamic Maxwell-plasma model are applied to simulate the linear and nonlinear optical response from SRR arrays.

In this paper, we numerically study the solution of the hydrodynamic electron fluid Maxwell equations by solving the electron density and momentum equations using an explicit finite difference hyperbolic PDE solver together with the FDTD method for the Maxwell's equations. This work is the extension of the previous work in [7,8] to electron fluid equations containing both electron density equation and the electron current equations with the electron pressure term included. We apply our model to simulate the nonlinear optical responses such as second-harmonic generation (SHG) from metallic nanoparticles and the numerical results yield good agreement with the experimental results published in [3–5].

2. Numerical Model of Hydrodynamic Electron Fluid Maxwell Equations

The hydrodynamic electron fluid Maxwell equations consists of the Maxwell's equations

$$\begin{aligned} \mu_0 \frac{\partial H}{\partial t} &= -\nabla \times E \\ \epsilon_0 \frac{\partial E}{\partial t} &= \nabla \times H - J \\ \nabla \cdot B &= 0 \\ \epsilon_0 \nabla \cdot E &= \rho \end{aligned} \tag{1}$$

and the hydrodynamic electron fluid equations

$$\frac{\partial n_e}{\partial t} + \nabla \cdot (n_e u_e) = 0 \tag{2}$$

$$\frac{\partial u_e}{\partial t} + (u_e \cdot \nabla) u_e + \gamma u_e = \frac{q_e}{m_e}(E + u_e \times B) - \frac{\nabla p}{m_e n_e} \tag{3}$$

where ϵ_0 and μ_0 represent vacuum permittivity and vacuum permeability, respectively. n_e, u_e, m_e and q_e are the electron density, velocity, electron mass and electron charge, respectively. The damping factor γ is added to describe the current decay due to Coulomb scattering. Equation (2) is the continuity equation and Equation (3) is the equation of motion (momentum conservation). p is the quantum pressure given by Thomas-Fermi theory,

$$p = \zeta (n_e)^{\frac{5}{3}}$$

where $\zeta = (3\pi^2)^{2/3}\hbar^2/5m_e$.

From Equations (2) and (3) we get

$$\frac{\partial (u_e n_e)}{\partial t} + \nabla \cdot (u_e \otimes (n_e u_e)) + \frac{\nabla p}{m_e} + \gamma u_e n_e = \frac{q_e}{m_e}(n_e E + n_e u_e \times B). \tag{4}$$

Let $n = q_e n_e$, and current density $J = q_e n_e u_e = n u_e$, which can be written as nonlinear hyperbolic system in conservation form

$$\frac{\partial n}{\partial t} + \nabla \cdot J = 0 \tag{5}$$

$$\frac{\partial J}{\partial t} + \nabla \cdot (\frac{J}{n} \otimes J + \frac{\zeta (q_e)^{-2/3} n^{5/3}}{m_e} I) + \gamma J = \frac{q_e}{m_e}(nE + J \times B) \tag{6}$$

where $\otimes$ is the tensor product.

For convenience, we rewrite the above system into the following conservation form

$$\frac{\partial m}{\partial t} + \frac{\partial F(m)}{\partial x} + \frac{\partial G(m)}{\partial y} + \frac{\partial K(m)}{\partial z} = S \tag{7}$$

where

$$m = \begin{pmatrix} n \\ J_x \\ J_y \\ J_z \end{pmatrix}, \; F(m) = \begin{pmatrix} J_x \\ \frac{J_x^2}{n} + \frac{\zeta (q_e)^{-2/3}}{m_e} n^{5/3} \\ \frac{J_y J_x}{n} \\ \frac{J_z J_x}{n} \end{pmatrix}, \; G(m) = \begin{pmatrix} J_y \\ \frac{J_x J_y}{n} \\ \frac{J_y^2}{n} + \frac{\zeta (q_e)^{-2/3}}{m_e} n^{5/3} \\ \frac{J_z J_y}{n} \end{pmatrix}$$

$$K(m) = \begin{pmatrix} J_z \\ \frac{J_x J_z}{n} \\ \frac{J_y J_z}{n} \\ \frac{J_z^2}{n} + \frac{\zeta (q_e)^{-2/3}}{m_e} n^{5/3} \end{pmatrix}, \; S = \begin{pmatrix} 0 \\ \frac{q_e}{m_e}(nE_x + J_y B_z - J_z B_y) - \gamma J_x \\ \frac{q_e}{m_e}(nE_y + J_z B_x - J_x B_z) - \gamma J_y \\ \frac{q_e}{m_e}(nE_z + J_x B_y - J_y B_x) - \gamma J_z \end{pmatrix}.$$

In this paper, we apply the standard space and time staggered grid based FDTD method to solve the Maxwell's Equation (1) and a non-staggered grid based central difference method to solve the hyperbolic Equation (7).

The FDTD Method is based on the space-time staggered Cartesian grid. The three components of the electric fields and the three components of the magnetic fields are defined at different positions in space and time. The electric fields are defined at the time step of τ; the magnetic fields are defined at the time step of $\tau + 1/2$. In a computational cell (i, j, k), three components of electric fields, E_x, E_y, and E_z, are defined at the locations of $(i + 1/2, j, k)$, $(i, j + 1/2, k)$, and $(i, j, k + 1/2)$, respectively; three components of magnetic fields, H_x, H_y, and H_z, are defined at the locations of $(i, j + 1/2, k + 1/2)$, $(i + 1/2, j, k + 1/2)$, and $(i + 1/2, j + 1/2, k)$, respectively. Since the current density J is defined at the same location as E in space and at the same location as H in time, our numerical method requires all components of J to be interpolated at cell corners. Hence, we define new variables j_x, j_y, j_z at cell corners such that

$$j_x(i, j, k) = (J_x(i + \tfrac{1}{2}, j, k) + J_x(i - \tfrac{1}{2}, j, k))/2 \tag{8}$$

$$j_y(i, j, k) = (J_y(i + \tfrac{1}{2}, j, k) + J_y(i, j - \tfrac{1}{2}, k))/2 \tag{9}$$

$$j_z(i, j, k) = (J_z(i, j, k + \tfrac{1}{2}) + J_z(i, j, k - \tfrac{1}{2}))/2. \tag{10}$$

We use the central difference method for solving the Equation (7), and its discretization form is given as

$$\begin{aligned} m^{\tau+\frac{1}{2}}(i,j,k) = m^{\tau-\frac{1}{2}}(i,j,k) + \Delta t S^{\tau}(i,j,k) \\ - \frac{\Delta t(F^{\tau-\frac{1}{2}}(i+1,j,k) - F^{\tau-\frac{1}{2}}(i-1,j,k))}{2\Delta x} \\ - \frac{\Delta t(G^{\tau-\frac{1}{2}}(i,j+1,k) - G^{\tau-\frac{1}{2}}(i,j-1,k))}{2\Delta y} \\ - \frac{\Delta t(K^{\tau-\frac{1}{2}}(i,j,k+1) - K^{\tau-\frac{1}{2}}(i,j,k-1))}{2\Delta z}. \end{aligned} \tag{11}$$

In the update Equation (11),

$$m^{\tau+\frac{1}{2}}(i,j,k) = \begin{pmatrix} n^{\tau+\frac{1}{2}}(i,j,k) \\ j_x^{\tau+\frac{1}{2}}(i,j,k) \\ j_y^{\tau+\frac{1}{2}}(i,j,k) \\ j_z^{\tau+\frac{1}{2}}(i,j,k) \end{pmatrix}.$$

When getting the value of j_x, j_y and j_z, we average them to get the value of J_x, J_y, and J_z as follows:

$$J_x(i+\frac{1}{2},j,k) = (j_x(i,j,k) + j_x(i+1,j,k))/2 \tag{12}$$

$$J_y(i,j+\frac{1}{2},k) = (j_y(i,j,k) + j_y(i,j+1,k))/2 \tag{13}$$

$$J_z(i,j,k+\frac{1}{2}) = (j_z(i,j,k) + j_z(i,j,k+1))/2. \tag{14}$$

Therefore, we have

$$j_x(i,j,k) = (j_x(i+1,j,k) + 2j_x(i,j,k) + j_x(i-1,j,k))/4 \tag{15}$$

$$j_y(i,j,k) = (j_y(i,j+1,k) + 2j_y(i,j,k) + j_y(i,j-1,k))/4 \tag{16}$$

$$j_z(i,j,k) = (j_z(i,j,k+1) + 2j_z(i,j,k) + j_z(i,j,k-1))/4 \tag{17}$$

which has filtering effect. Our numerical simulations show that the above central difference method provides stable solution.

3. Numerical Simulation of SHG from SRR

In this section, we simulate the optical second-harmonic generation (SHG) from metallic nanoparticles numerically using the numerical solver presented in the previous section. The simulation results are compared with optical experimental results shown in the paper [3–5]. The simulation setup is shown in Figure 1a. The red arrow represents the direction of incident pulse; the blue arrow represents the direction of second harmonic waves. A three-dimensional gold nanoparticle is placed in the middle of the computational domain with periodic boundary conditions in both x and y directions. Perfectly Matched Layers boundary condition is applied in z direction. The gold nanoparticle is U-shaped with plasma frequency $\omega_p = 1.367 \times 10^{16} s^{-1}$ and phenomenological damping factor $6.476 \times 10^{13} s^{-1}$, and thickness of $25\ nm$. The $x-y$ cross section of the U-shaped gold nanostructure is shown in

Figure 1b. ITO ($\epsilon = 3.8$ and $5\ nm$ thick) and glass ($\epsilon = 2.25$ below ITO to the bottom) substrates are placed beneath the particle. The rest of the computational domain is vacuum.

The incident Gaussian pulse with carrier wavelength $\lambda = 1500\ nm$ is excited in x direction and propagates along z-axis. Its profile is given by

$$E_x^{\text{inc}} = E_0 \sin\left(\frac{2\pi c}{\lambda} t\right) \exp\left(-\frac{(t - 6t_0)^2}{t_0^2}\right) \tag{18}$$

where $t_0 = 20\ fs$. The strength of the incident pulse is $E_0 = 2 \times 10^7\ V/m$. The energy conversion efficiency of the SHG is defined by

$$\eta = \sqrt{\epsilon_{sub}} \left| \frac{E_y(2\omega)}{E_x(\omega)} \right|^2 \tag{19}$$

where E_x represents the incident pulse, E_y is the second-harmonic signal, ϵ_{sub} is the dielectric permittivity of the substrate.

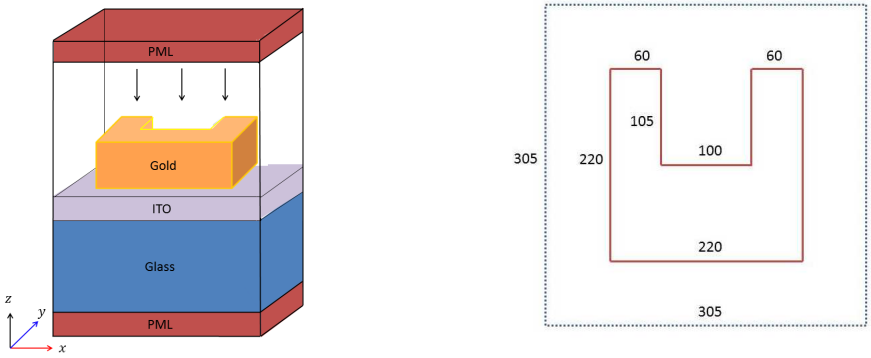

(a) **(b)**

Figure 1. (**a**) The computational domain for optical pulse propagation through three dimensional gold nanostructures; (**b**) $x - y$ cross-section of the U-shaped gold nanostructure with the unit of nm.

In our numerical simulations, we choose uniform grids given by $\Delta x = \Delta y = \Delta z = 2.5\ nm$ and $\Delta t = 4.167 \times 10^{-18} s$ according to the Courant-Friedrichs-Lewy condition number of 0.5.

Figure 2a shows the time history of linear (E_x) and nonlinear second harmonic (E_y) waves for U-shaped metallic particles illuminated by x-polarized incident light. In Figure 3, the wavelengths of E_x and E_y components are plotted after the Fourier transform. The conversion efficiency in our numerical simulation is calculated as 1.3959×10^{-11} which is in good agreement with the experimental result (less than 2×10^{-11} as published in [4,5]). Good agreements are achieved between our numerical result and the experimental result.

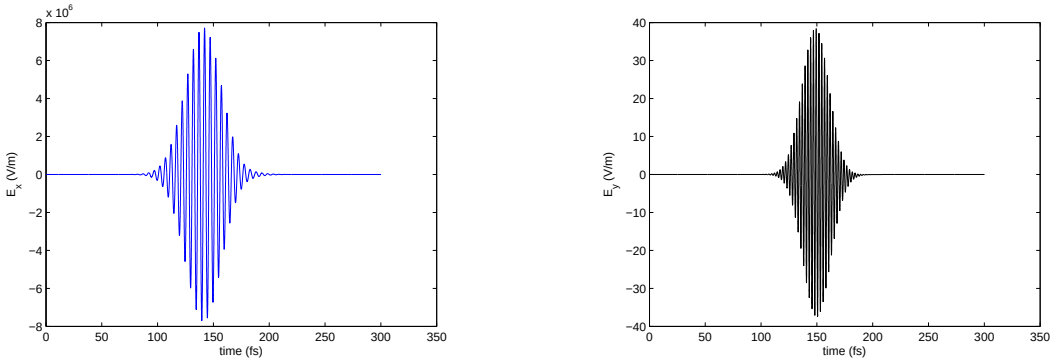

(a) **(b)**

Figure 2. Time history of (**a**) the linear response, and (**b**) the nonlinear response, for U-shaped metallic particles illuminated by a x-polarized incident light.

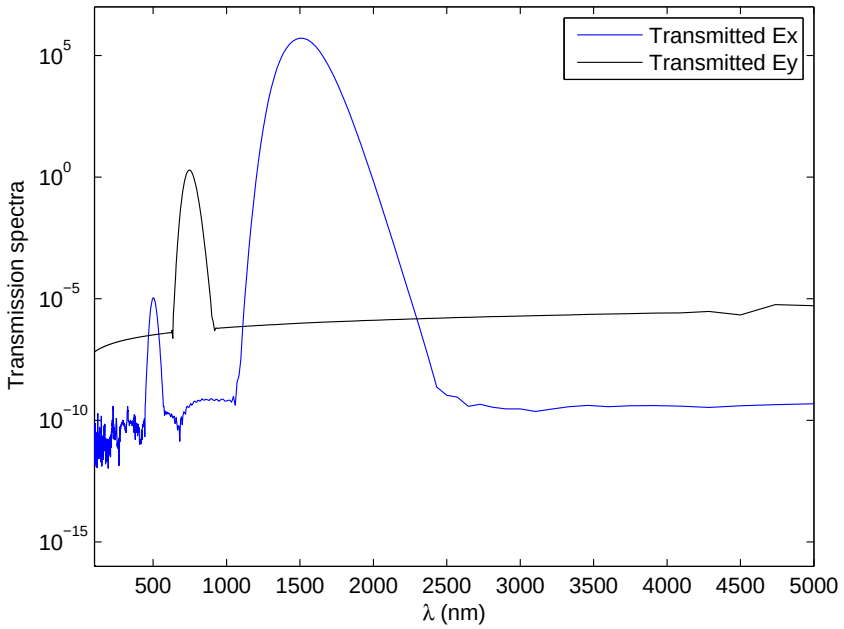

Figure 3. Semi-log plot of the Fourier transform of the time history of the far-field projection of the E_x and E_y components of the electric field as functions of the wavelength for U-shaped nanoparticles illuminated by a x-polarized incident light.

In the second simulation, we test our model for a rectangular shaped nanoparticle, and the corresponding results are shown in Figure 4. The structure is similar to the rectangular shaped structure given in [4]. Since rectangular shaped structure is symmetric in both x and y directions, there is no SHG, but there exists third harmonic generation (THG). Experimental results on third harmonic generation were published in [4]. As shown in Figure 4, our results confirm that no SHG is generated from rectangular nanoparticles and there is THG for both U-shaped (shown in Figure 2) and rectangular shaped structures. The SHG from U-shape is much stronger than the rectangular shape, which is also in agreement with the experimental results published in [4].

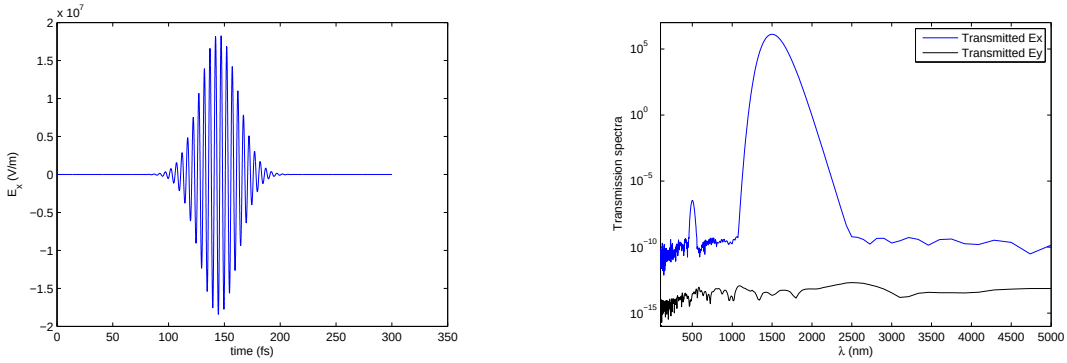

(a) **(b)**

Figure 4. (**a**) Time history of the linear response for rectangular shaped nanoparticle illuminated by a x-polarized incident light; (**b**) Semi-log plot of the Fourier transform of the time history of the far-field projection of the E_x and E_y components of the electric field as functions of the wavelength.

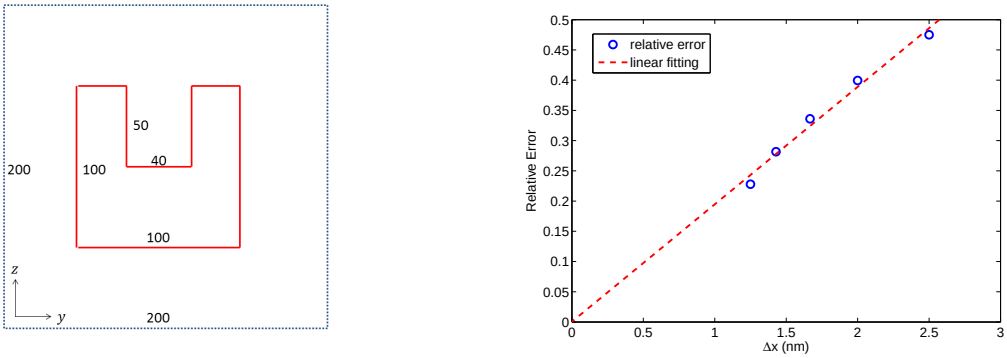

(a) **(b)**

Figure 5. (**a**) $y-z$ cross-sections of the U-shaped gold nanostructure with the unit of nm; (**b**) the convergence test of the our numerical method for solving SHG strength.

Furthermore, we test the convergence of our method using a smaller two dimensional structure shown in Figure 5a. The U-shaped nanostructure is in $y-z$ plane and infinitely long in the x-direction. We use a uniform grid whose size varies from 2.5 nm down to 1.25 nm. A fine grid result with $\Delta x = 0.625\ nm$ is chosen as the reference solution. From the convergence test result shown in Figure 5b, we conclude that our numerical method is convergent.

4. Conclusions

We have investigated the numerical solution of three-dimensional hydrodynamic electron fluid Maxwell equations. Our numerical method is based on the Finite-Difference Time-Domain (FDTD) method for solving the Maxwell's equations and central difference method for the hydrodynamic electron fluid equations. We apply our method to study the second-harmonic generation (SHG) from metallic nanoparticles (the split ring-resonator). The conversion efficiency obtained by our numerical method is in good agreement with the previously published experimental result.

Acknowledgments

We thank Moysey Brio and Yong Zeng for invaluable discussions. This work was supported in part by the US ARO Grant W911NF-11-2-0046, and NSF Grant HRD-1242067.

Author Contributions

YZ and JL developed the algorithm; YZ wrote the computer program and performed the computer simulation; YZ wrote the paper.

Conflicts of Interest

The authors declare no conflict of interest.

References

1. Jackson, J.D. *Classical Electrodynamics*, 2nd ed.; Wiley: New York, NY, USA, 1975.
2. Taflove, A.; Hagness, S. *Computational Electrodynamics: The Finite-Difference Time-Domain Method*, 3rd ed.; Artech House: Norwood, MA, USA, 2005.
3. Klein, M.W.; Enkrich, C.; Wegener, M.; Linden, S. Second-Harmonic Generation from Magnetic Metamaterials. *Science* **2006**, *313*, 502–504.
4. Klein, M.W.; Wegener, M.; Feth, N.; Linden, S. Experiments on second- and third-harmonic Generation from Magnetic Metamaterials. *Opt. Express* **2007**, *15*, 5238–5247.
5. Klein, M.W.; Wegener, M.; Feth, N.; Linden, S. Experiments on second- and third-harmonic Generation from Magnetic Metamaterials: erratum. *Opt. Express* **2008**, *16*, 8055.
6. Feth, N.; Linden, S.; Klein, M.W.; Decker, M.; Niesler, F.B.P.; Zeng, Y.; Hoyer, W.; Liu, J.; Koch, S.W.; Moloney, J.V.; *et al.* Second-harmonic generation from complementary split-ring resonators. *Opt. Lett.* **2008**, *33*, 1975–1977.
7. Zeng, Y.; Hoyer, W.; Liu, J.; Koch, S.W.; Moloney, J.V. A classical theory for second-harmonic generation from metallic nanoparticles. *Phys. Rev. B* **2009**, *79*, 235109.
8. Liu, J.; Brio, M.; Zeng, Y.; Zakharian, A.; Hoyer, W.; Koch, S.W.; Moloney, J.V. Generalization of the FDTD algorithm for simulations of hydrodynamic nonlinear Drude model. *J. Comput. Phys.* **2010**, *229*, 5921–5932.
9. Ciracì, C.; Poutrina, E.; Scalora, M.; Smith, D.R. Origin of second-harmonic generation enhancement in optical split-ring resonators. *Phys. Rev. B* **2012**, *85*, 201403.

10. Ciracì, C.; Poutrina, E.; Scalora, M.; Smith, D.R. Second-harmonic generation in metallic nanoparticles: Clarification of the role of the surface. *Phys. Rev. B* **2012**, *86*, 115451.
11. Grynko, Y.; Meier, T.; Linden, S.; Niesler, F.B.P.; Wegener, M.; Förstnera, J. Optimal Second-Harmonic Generation in Split-Ring Resonator Arrays. *Proc. SPIE* **2013**, doi:10.1117/12.2003279.